Computational and Structural Biotechnology Journal 25 (2024) 95–104

Contents lists available at ScienceDirect

Computational and Structural Biotechnology Journal

journal homepage: www.elsevier.com/locate/csbj

Numerical simulation study of nanoparticle diffusion in gray matter

Peiqian Chen [a,b], Bing Dong [c], Weiwu Yao [a,b,*]

[a] Tongren Hospital, No. 1111, Xianxia Rd., Shanghai, China
[b] School of Medicine, Shanghai Jiao Tong University, No. 280, South Chongqing Rd., Shanghai, China
[c] School of Nuclear Science and Engineering, Shanghai Jiao Tong University, No. 800, Dongchuan Rd., Shanghai, China

A B S T R A C T

Purpose: Nanomedicine-based approaches have shown great potential in the treatment of central nervous system diseases. However, the fate of nanoparticles (NPs) within the brain parenchyma has not received much attention. The complexity of the microstructure of the brain and the invisibility of NPs make it difficult to study NP transport within the grey matter. Moreover, regulation of NP delivery is not fully understood.
Methods: 2D interstitial system (ISS) models reflecting actual extracellular space (ECS) were constructed. A particle tracing model was used to simulate the diffusion of the NPs. The effect of NP size on NP diffusion was studied using numerical simulations. The diffusion of charged NPs was explored by comparing experimental and numerical simulation data, and the effect of cell membrane potential on the diffusion of charged NPs was further studied.
Results: The model was verified using previously published experimental data. Small NPs could diffuse efficiently into the ISS. The diffusion of charged NPs was hindered in the ISS. Changes in cell membrane potential had little effect on NP diffusion.
Conclusion: This study constructed 2D brain ISS models that reflected the actual ECS and simulated the diffusion of NPs within it. The study found that uncharged small NPs could effectively diffuse within the ISS and that the cell membrane potential had a limited effect on the diffusion of charged NPs. The model and findings of this study can aid the design of nanomedicines and nanocarriers for the diagnosis and treatment of brain diseases.

1. Introduction

Nanomedicine aims to apply nanotechnology to the prevention, imaging, diagnosis, monitoring, and treatment of diseases [1,2,3]. Although nanomedicine is still in its early stages, many applications have been developed. In the central nervous system, nanodrugs are used to treat Alzheimer's disease, glioma, stroke, Parkinson's disease, and other diseases [4,5]. Because of the blood-brain barrier (BBB) and blood-cerebrospinal fluid barrier, it is difficult for most traditional drugs to enter the brain parenchyma. Nanoparticles (NPs), owing to their small size and high surface area-to-volume ratio, can successfully cross the BBB with reasonable modification. The development and application of nanodrug delivery systems which can cross the BBB are popular research topics. However, little attention has been paid to the fate of NPs after they cross the BBB, that is, their transport in the brain parenchyma.

Substance transport in brain parenchyma occurs via the interstitial system (ISS). The brain ISS is a nanoscale network of continuously connected tubes and slices that surround each nerve cell [6]. The brain ISS contains interstitial fluid and the extracellular matrix (ECM), which usually account for 15–30 % of the brain volume, that is, the volume fraction (α) is 15–30 % [7]. The ISS plays many roles in brain function such as cell maintenance and adhesion, communication among neural cells, information processing and integration, and coordinated responses to changes in the external and internal environments of the brain [8]. The transport of NPs in the ISS is inevitably affected by their characteristics and the external environment. Thorne and Nicholson used comprehensive optical imaging technology to predict the width of the extracellular space (ECS) in living tissue by obtaining the diffusion coefficients of NPs of different sizes in the rat cerebral cortex, and clarified the size limit of NPs that could be diffused in the brain [9]. Lieleg et al. experimentally confirmed that the diffusion of positively or negatively charged micrometre particles and NPs was markedly limited in the ECM, whereas uncharged particles easily diffused [10]. Nanoparticles moving through the ISS may combine with cell membranes and affect the cells. Warren and Payne found that NPs with amine-modified surfaces cause significant depolarisation of CHO and HeLa cells by blocking ion channels [11]. Dante et al. found that low concentrations of negatively charged NPs could interact with neuronal membranes and synaptic clefts, whereas positively and neutrally charged NPs were not localised to neurones. The presence of negatively charged NPs on neuronal membranes affects neuronal excitability by increasing the amplitude and frequency of spontaneous postsynaptic currents at the single-cell level and increasing spiking activity and synchronised firing at the neural network level [12]. In summary, different NPs move differently

* Corresponding author at: Tongren Hospital, No. 1111, Xianxia Rd., Shanghai, China.
E-mail address: yaoweiwuhuan@163.com (W. Yao).

https://doi.org/10.1016/j.csbj.2024.06.002
Received 1 March 2024; Received in revised form 2 June 2024; Accepted 4 June 2024
Available online 10 June 2024
2001-0370/© 2024 Published by Elsevier B.V. on behalf of Research Network of Computational and Structural Biotechnology. This is an open access article under the CC BY-NC-ND license (http://creativecommons.org/licenses/by-nc-nd/4.0/).

in the ISS and affect cells. Despite the importance of exploring the transport properties of NPs in the ISS, systematic studies on the transport of NPs in the ISS are few.

Although the preparation of NPs and conducting biological experiments are the common research methods, numerical simulation is an alternative method that can systematically study the transport of NPs, having the advantages of low cost, high speed, and precision; most importantly, it allows an understanding of the mechanical environment that is usually inaccessible. Yuan et al. simulated the diffusion of NPs in the brain white matter by establishing a stochastic geometric model and a mathematical particle tracking model, and found that for negatively charged NPs, the particle size and surface charge were positively correlated with the diffusion coefficient (D) before reaching the threshold [13]. Hansing et al. proposed a simple model for the diffusion of charged NPs in cross-linked charged hydrogels and confirmed that electrostatic interactions were a key factor influencing the diffusivity of charged NPs and that oppositely charged gels were much more effective in slowing down charged particles than similarly charged gels [14]. However, none of the current ISS models can fully restore actual ISS geometry.

In the present study, 2D ISS models were constructed based on the electron microscopy (EM) images of samples prepared by high-pressure cryofixation, and a mathematical particle tracking model was utilised to simulate the diffusion of NPs. First, the models used in this study were validated by comparison with data from the literature. The effect of NP size on NP diffusion was investigated using numerical simulations. Finally, the diffusion of charged NPs in the ISS was explored by comparing experimental and numerical simulation data, and the effect of cell membrane potential on the diffusion of charged nanoparticles was further studied. The results obtained in this study can aid in the development of nanomedicines for the diagnosis and treatment of brain disorders.

2. Methods and materials

2.1. Numerical simulation

Diffusion and advection are the two mechanisms of substance transport in fluids. In the ISS, diffusion rather than advection plays a major role in the transport of substances [15,16]. Therefore, the present study only considers NP diffusion in the ISS and ignores the effect of advection.

2.1.1. Geometry and mesh

Electron microscopy offers unparalleled capabilities for studying cellular morphology and structure at nanoscale resolution. Compared to chemical fixation, high-pressure cryofixation can preserve samples in a near-native state. Therefore, high-pressure cryofixation can preserve physiological extracellular space [17]. Tsang et al. processed mouse brain slices using the CryoChem method and characterised them using serial block-face scanning EM and 3D correlated light and electron microscopy [18]. In the present study, five EM images of the mouse hypothalamus (a small grey matter structure) were randomly intercepted from the study by Tsang et al. (avoiding somas of nerve cells). Then, the 2D ISS geometry was manually outlined after identifying the cells and extracellular space, as shown in Fig. 1A-C. The geometric diagrams of the five ISS models are shown in Fig. S1.

After establishing the ISS geometry, a mesh was established for the particle tracking simulation. An automatically generated triangular mesh was used in the model, as shown in Fig. 1D-E. Subsequently, a

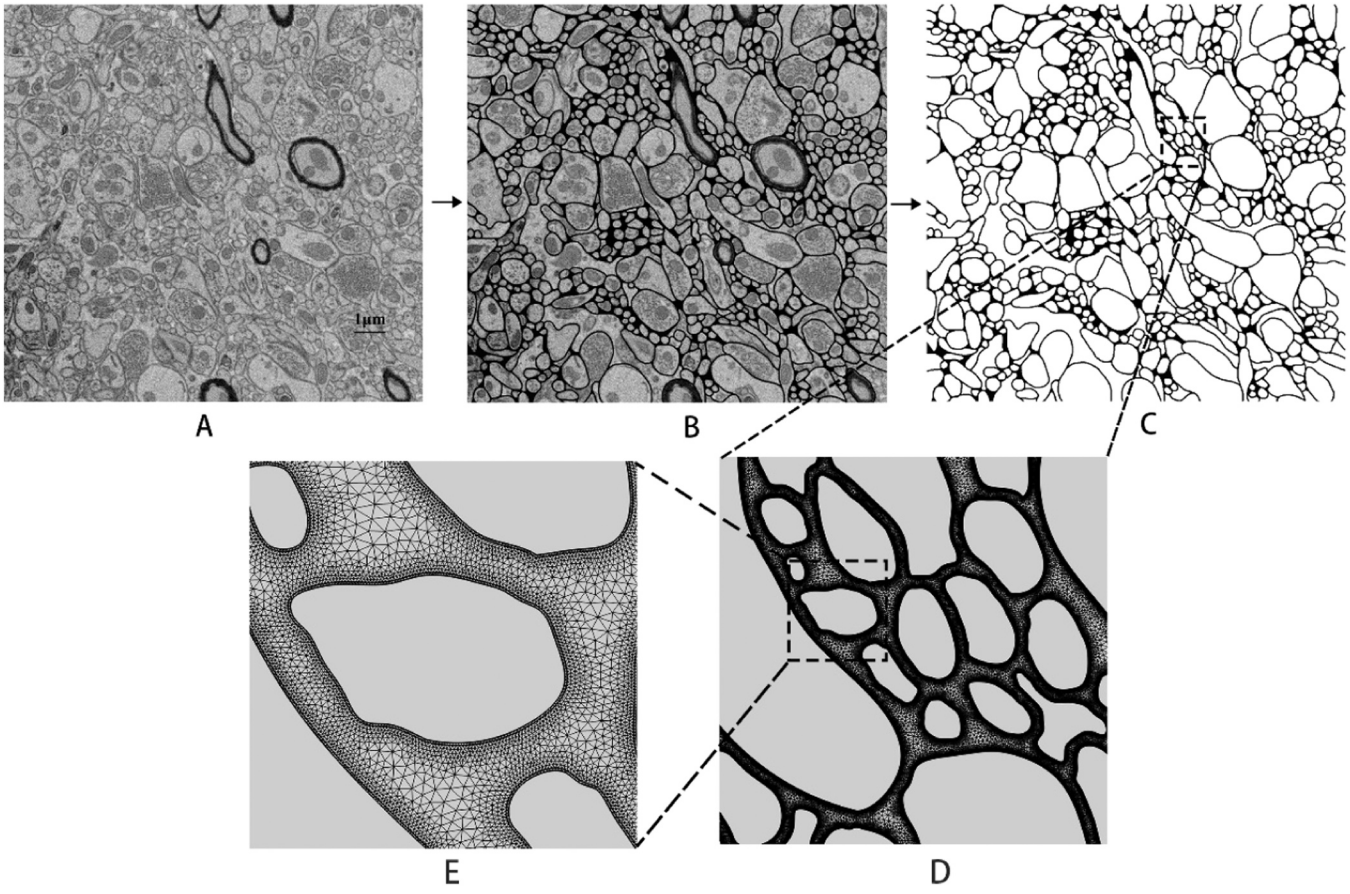

Fig. 1. 2D interstitial system (ISS) model construction and mesh. A. Original electron micrograph. B. Manually outlined ISS network. C. Extracted ISS geometry. D. Mesh for the geometry. E. Detailed view of the mesh.

mesh sensitivity analysis was performed. The mesh was refined three times. When more than 10 elements were present in the gap between the two cells, the result was independent of the mesh refinement. Finally, the number of elements in the five ISS models were 2801015, 2840054, 2612275, 2873949, and 2865539. The average quality of the mesh was 0.8117, 0.8066, 0.828, 0.8143, and 0.8156, respectively, which was sufficient to ensure the convergence and accuracy of the simulation.

2.1.2. Mathematical model

Force on the particle.

The motion of NPs in the ISS can be described by Newton's second law:

$$m_p \frac{d^2\mathbf{x}}{dt^2} = \mathbf{F} \tag{1}$$

where x is the position of the particle (m), m_p is the particle mass (kg), and F is the sum of all forces acting on the particle (N).

When a single NP moves in the ISS, it is mainly affected by its own molecular thermal motion (Brownian motion), interaction with the ECM environment, particle-particle interaction, and cell membrane interaction.

Molecular thermal motion-Brownian force.

Brownian force is an important force for NP movements. The Brownian force originates from the unbalanced force exerted by the surrounding fluid molecules and can be expressed in a drag analogy force model under a Lagrangian reference frame. The Brownian force F_B is defined as follows:

$$F_B = \zeta \sqrt{\frac{6\pi k_B \mu T d_p}{\Delta t}} \tag{2}$$

where Δt is the time step in the calculation (s), μ is the dynamic viscosity of the fluid (Pa·s), T is the fluid temperature (K), k_B is the Boltzmann constant, d_p is the diameter of NP (m), and ζ is a normally distributed random number with a mean of zero and unit standard deviation.

Forces from the fluid environment-Drag force.

The drag force was used to model the viscous drag force acting on the particle owing to the presence of the ECM, which is defined as

$$\mathbf{F}_D = \left(\frac{1}{\tau_p}\right) m_p (\mathbf{u} - \mathbf{v}) \tag{3}$$

where τ_p is the particle velocity response time (s), $\mathbf{v}$ is the particle velocity (m/s), and $\mathbf{u}$ is the fluid velocity (m/s).

Stokes drag law was applied in the simulation because of the low relative Reynolds number. According to the Stokes drag law, the velocity response time is calculated as $\tau_p = \frac{\rho_p d_p^2}{18\mu}$ (4).

where μ is the fluid viscosity (Pa·s), ρ_p is the particle density (kg/m^3), and d_p is the particle diameter (m).

Particle-particle interaction.

The NPs were diluted in this study; therefore, hard collisions between particles were ignored. The interaction between the charged nanoparticles was simulated by the Coulomb force, which is defined as

$$\mathbf{Fc} = \frac{e^2}{4\pi\epsilon_0} \sum_{j=1}^{N} ZZ_j \frac{\mathbf{r} - \mathbf{r}_j}{|\mathbf{r} - \mathbf{r}_j|^3} \tag{5}$$

where ϵ_0 is the vacuum permittivity (F/m), e is the charge quantity of one particle (C), and $\mathbf{r}$ and $\mathbf{r}_j$ stand for the position of the two particles (m).

According to Eq. (5), the calculation of the Coulomb force between

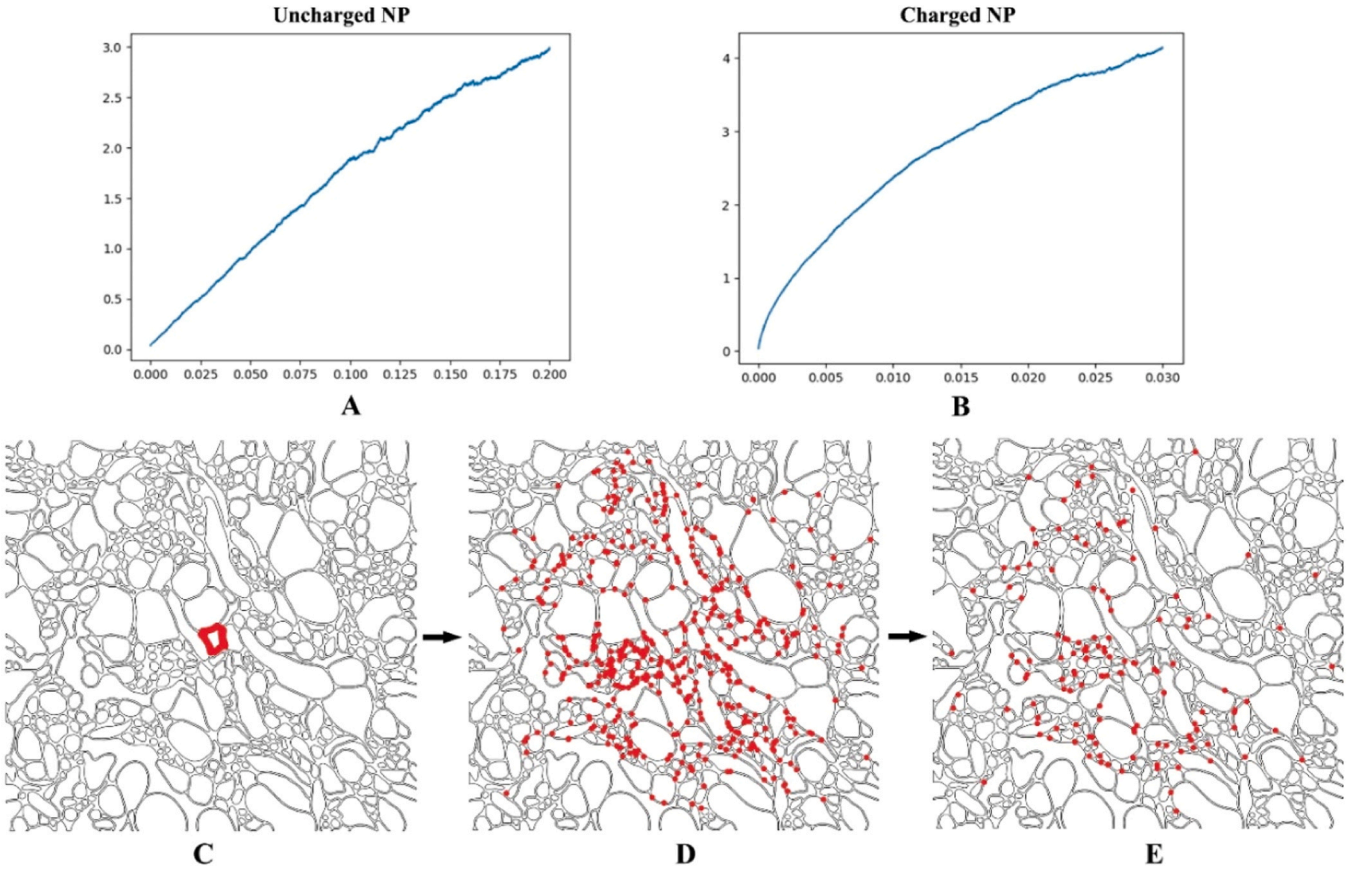

Fig. 2. Release of nanoparticles (NPs). The typical time-R^2 curves of uncharged (A) and charged (B) NPs. C. NPs are released at the centre of the model. D. NPs diffuse steadily. E. NPs begin to leave the domain.

NPs requires the charged quantity of a single particle. However, the charged quantity of a single NP cannot be directly measured. The present study refers to the research method of Yuan et al., who used the zeta potential (Zp) to describe the charged quantity of NPs [13]. Ge et al. successfully estimated the nanodiamond surface charge density from its measured Zp and determined the relationship between the effective surface charge density and the actual surface charge density of the nanodiamond [19]. Yuan et al. adopted this relationship to describe the effective charge density of NPs more precisely as follows:

$$\delta_{\text{eff}} = \sqrt{8cN\epsilon k_B T}\sinh\frac{e\zeta}{2k_B T} \tag{6}$$

where δ_{eff} is the effective charge density (C/m^3), c represents the ion concentration (mol/L), ϵ is the permittivity of the solution (F/m), N is the Avogadro constant (mol^{-1}), and ζ is the Zp of the NP (V).

Force from cell membrane.

The configuration of ion transporters in the cell membrane and the concentration of ions in the fluid on both sides of the cell membrane cause a difference in the total charge inside and outside the cell membrane, that is, the membrane potential. In neurones, the resting potential has a value of approximately − 70 mV. When charged NPs move into the active range of cell membranes, particle-surface interactions become significant. The Derjaguin, Landau, Verwey, and Overbeek theory can be used to describe the interaction between a particle and a plate [20]. When a charged NP enters the active range of the cell membrane, the force on the particle is the sum of the van der Waals and electric double-layer forces. Electrostatic interactions are the same as van der Waals forces, either repulsive or attractive, but are stronger and occur over greater distances than van der Waals forces [21]. To simplify the model, the present study used the Coulomb force to simulate the electric double-layer force of the cell membrane on the charged NPs by setting the membrane potential cut-off and ignoring the van der Waals force between the NPs and the cell membrane.

In a study of the interaction between NPs and cell membranes simulated by molecular dynamics, the cut-off length of the Coulombic potential was set to 0.9–1.2 nm [22,23]. However, the 1.2 nm cut-off length is too small for the micron-scale model, which is difficult to manipulate in model construction. Therefore, in the present study, the range of the membrane potential was set to 3 nm, that is, the membrane potential smoothly shifted from 0 to 3 nm, as shown in Fig. 7B. Given that the size of NPs is several orders of magnitude smaller than that of the cells, the cell membrane can be treated as a flat plate [24]. Thus, the Gouy–Chapman equation (Eq. (7)) can be used to quantify the relationship between the surface charge density and surface electrostatic potential.

$$\delta = \sqrt{8cN\epsilon k_B T}\sinh\frac{e\Psi_0}{2k_B T} \tag{7}$$

where δ is the surface charge density (C/m^3) and Ψ_0 is the surface electrostatic potential of a flat charged surface (V).

In reality, when NPs are transported in the brain ISS, in addition to the above-mentioned forces, they are also affected by other factors, such as the composition of the ECM and the cellular uptake of NPs. However, the influence of these factors on the NP trajectories is too complex to be described and mathematically resolved within the current framework. These factors, which cannot be modelled mathematically, are treated as lumped systems, which means that, although each factor within the lumped system might manipulate the particle's motion in a specific manner, the overall effect of the system on each particle is the same [13].

2.1.3. Material properties

The parameters used in the present study, such as electrical conductivity, relative dielectric constant, and viscosity of the ECM are listed in Table 1.

2.1.4. Particle release and simulation setup

The NPs were released simultaneously in the centre of the model, within a circle having a radius of 0.46 μm, as shown in Fig. S1. The number of particles released was 900; this number of NPs was selected after sensitivity research, as being sufficient for obtaining statistically stable results. All simulations were performed on COMSOL Multiphysics® 6.0 software package. An iterative coupled solver was utilised for the membrane potential simulation, and a direct segregated solver was utilised for the particle tracking simulation. The simulations were run with an adaptive time step up to 0.1–0.5 s until some NPs left the domain. Relative tolerance in the simulation was 1×10^{-5}.

2.2. In vitro experiment

FITC@Fe_3O_4 was purchased from Beijing Zhongkeleiming Daojin Technology, Beijing, China. The transmission electron microscope and dynamic light scattering particle sizes of FITC@Fe_3O_4 were 10 nm and 20.41 nm, respectively. The Zp of FITC@Fe_3O_4 was − 22.4 mV. The iron concentration in FITC@Fe_3O_4 was 1 mg/mL. Male mice (C57BL/6 J, 8-week-old, 25 g) were purchased from Charles River Laboratories. Feeding and experimentation with the mice followed the regulations of the Ethics Committee of Shanghai Tongren Hospital (approval number 2021–075-01). To prepare 400 μm thick cortical slices, the mice were euthanized by cervical dislocation, and brain slices were prepared according to the protocol described in [26]. The brain slices were placed in a brain slice recording tank (RC-26 G, Warner Instruments) and fixed with an anchor (SHD-26GH/2, Warner Instruments), and artificial cerebrospinal fluid with oxygen at 37 ± 0.5 °C was continuously injected using a peristaltic pump (BT100–2 J, Longer). Fluorescence was captured with a 5 × microscope objective on an Olympus BX51WI

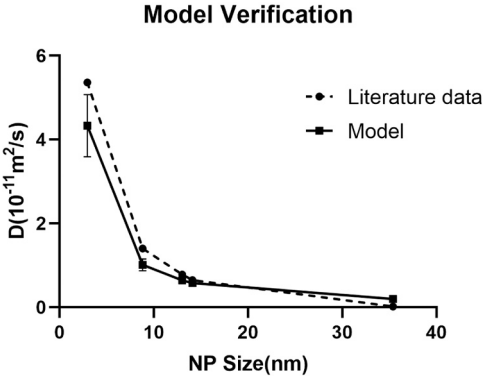

Fig. 3. Comparison of simulation results with literature data.

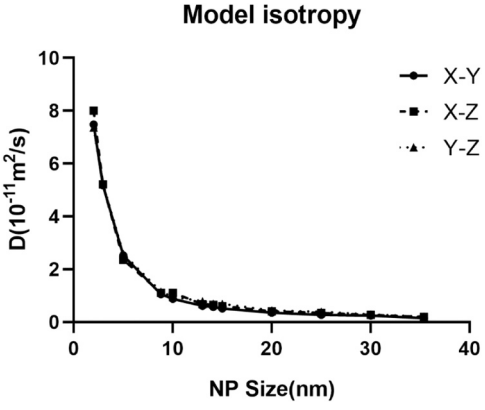

Fig. 4. Diffusion coefficient of 2–35 nm nanoparticles (NPs) in the X-Y, X-Z, and Y-Z directions.

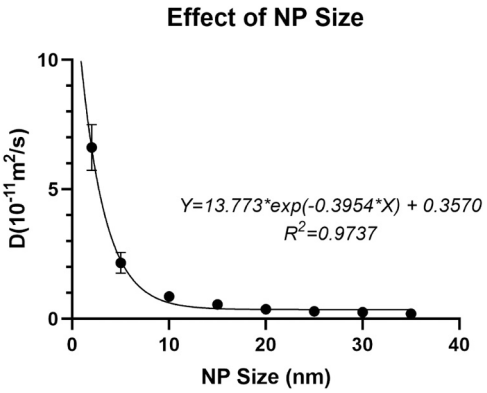

Fig. 5. Diffusion coefficients of uncharged nanoparticles (NPs) of different sizes.

microscope and imaged using a CCD camera (TUCSEN USB 2.0 H series) with an exposure time of 250 ms. A glass microelectrode containing suitable FITC@Fe_3O_4 with a tip diameter of 3–5 μm was inserted into the cortical region of the brain slice at an angle of 30° relative to the surface until the tip was in the middle of the slice (at a depth of approximately 200 μm). The glass electrode was connected to a pressure syringe pump (LSP01–1A, LSP Syringe Pump), and the injection pressure and duration were adjusted such that the volume of FITC@Fe_3O_4 was suitable for the sensitivity and dynamic range of the CCD camera. After spraying, a set of approximately 5–10 consecutive images was taken to document the diffusion process, as shown in Fig. 6B-F. The interval between two consecutive images was 1 min. After acquisition, the images were processed and analysed to extract the diffusion parameters using the method described in Section 2.3..

2.3. Particle diffusion in simulation and experiment

Particle diffusion is driven by the concentration gradient in the ISS. In the simulation, diffusion was studied from a microscopic perspective in which the Brownian force dominates the diffusion process and was modelled. In the experiment, diffusion was studied macroscopically, in which the concentration field was measured, and the diffusion coefficient was acquired from the concentration field.

The Einstein relation can be used to connect the microscopic particle movement and macroscopic diffusion coefficient. Mapping the macroscopic quantity (diffusion coefficient) to microscopic mechanisms (displacement of particles) requires obtaining the trajectory of each particle as the input. Eq. (8) is a general method for calculating the particle diffusion coefficients [27,28].

$$D_0 = < R^2 > / 4t$$
$$< R^2 > = \sum_{i=1}^{n} \left(dx_i^2 + dy_i^2 \right) \tag{8}$$

where D_0 is the diffusion coefficient of the particles (m^2/s), $< R^2 >$ is the average of mean squared displacement (MSD) of all the particles (m^2), t is the diffusion time (s), n is the number of NPs in the system, and dx and dy are the displacements of the particles in the x and y directions, respectively.

Because the displacement of particles in the simulation can be easily evaluated by post-processing, the procedure for obtaining the diffusion coefficient in the experiments is the most important, which is described as follows.

The particle diffusion in the experiments can be treated as the diffusion of the instantaneous point source. Assuming that the diffusion coefficient is isotropic, the concentration field is controlled by

$$\frac{\partial C}{\partial t} = D \frac{\partial^2 C}{\partial r^2} \tag{9}$$

The initial condition of Eq. (10) is:

$$C(r)\,|_{t=0} = M\delta(r) \tag{10}$$

where C is the concentration of the NPs at time t (kg/m^2), M is the initial mass of the point source (kg), $\delta(x)$ is the Dirac delta function, D is the diffusion coefficient (m^2/s), and r is the radial position (m).

Solving Eq. (9), the concentration field is theoretically calculated as follows:

$$C(r) = \frac{M}{4\pi Dt} \exp\left(-\frac{r^2}{4Dt} \right) \tag{11}$$

To acquire the diffusion coefficient of the NPs, a region of interest (ROI) was determined, in which the intensities of the pixels were used to interpolate the concentration field of the NPs. In this study, the ROI was a circle, the centre coordinates of which were acquired by finding the highest intensities of the pixels, and the radius was a constant value ranging from 200 to 300 pixels. The concentration field was constructed using least-squares interpolation.

After a series of concentration fields at various times were acquired in the experiments, two unknown variables, M and Dt were derived by least-squares interpolation according to Eq. (11), where Dt was the focus. Finally, the diffusion coefficient D can be derived by fitting the value of Dt to time t.

3. Results

3.1. Model verification

The dimension of the five models were all 13.42 × 12.73 μm^2, and the ISS areas were 40.21 μm^2, 46.48 μm^2, 31.34 μm^2, 37.29 μm^2, and 36.59 μm^2. The volume fraction (α) of the five models ranged from 18.35 % to 27.21 %, which was consistent with the fact that α was 15–30 % under physiological conditions [7].

The typical time-R^2 curves of the uncharged and charged NPs are shown in Fig. 2A-B. The diffusion coefficient D was obtained from Eq. (8), that is, the slope of the line in the stable diffusion stage. The simulated results were compared with the results obtained in [9,29], as shown in Fig. 3 and Table 2. The simulation results for the 13 nm NPs and 14 nm NPs were consistent with the experimental results. The simulation results of 2.95 nm NPs and 8.8 nm NPs were slightly lower than the experimental measurements, and the simulated result of 35 nm NPs was slightly higher than the experimental measurements. Overall, the simulation results were in good agreement with the experimental results. As a geometric model of the NPs was not constructed, the space occupation of the NPs was ignored. In the real world, 35 nm NP are considerably hindered when diffusing in an ISS channel with a similar diameter. Therefore, this model is suitable for NPs in the range of 2–35 nm. The simulation of NP diffusion outside this range may deviate from real world conditions.

Simulation and experimental data were expressed as mean ± standard deviation.

3.2. Model isotropy

To explore whether there were any differences in the diffusion coefficients of the NPs in different directions, we randomly selected one model from the five models, taking the centre of its original EM image in the X-Y direction as the origin, and used IMOD software (Boulder Colorado) to reconstruct the EM images in the X-Z and Y-Z directions. The ISS models in the X-Y, X-Z, and Y-Z directions were then constructed, and a simulation of NP diffusion was performed, as shown in Fig. S2. In this experiment, the diffusion of uncharged NPs (2–35 nm) was

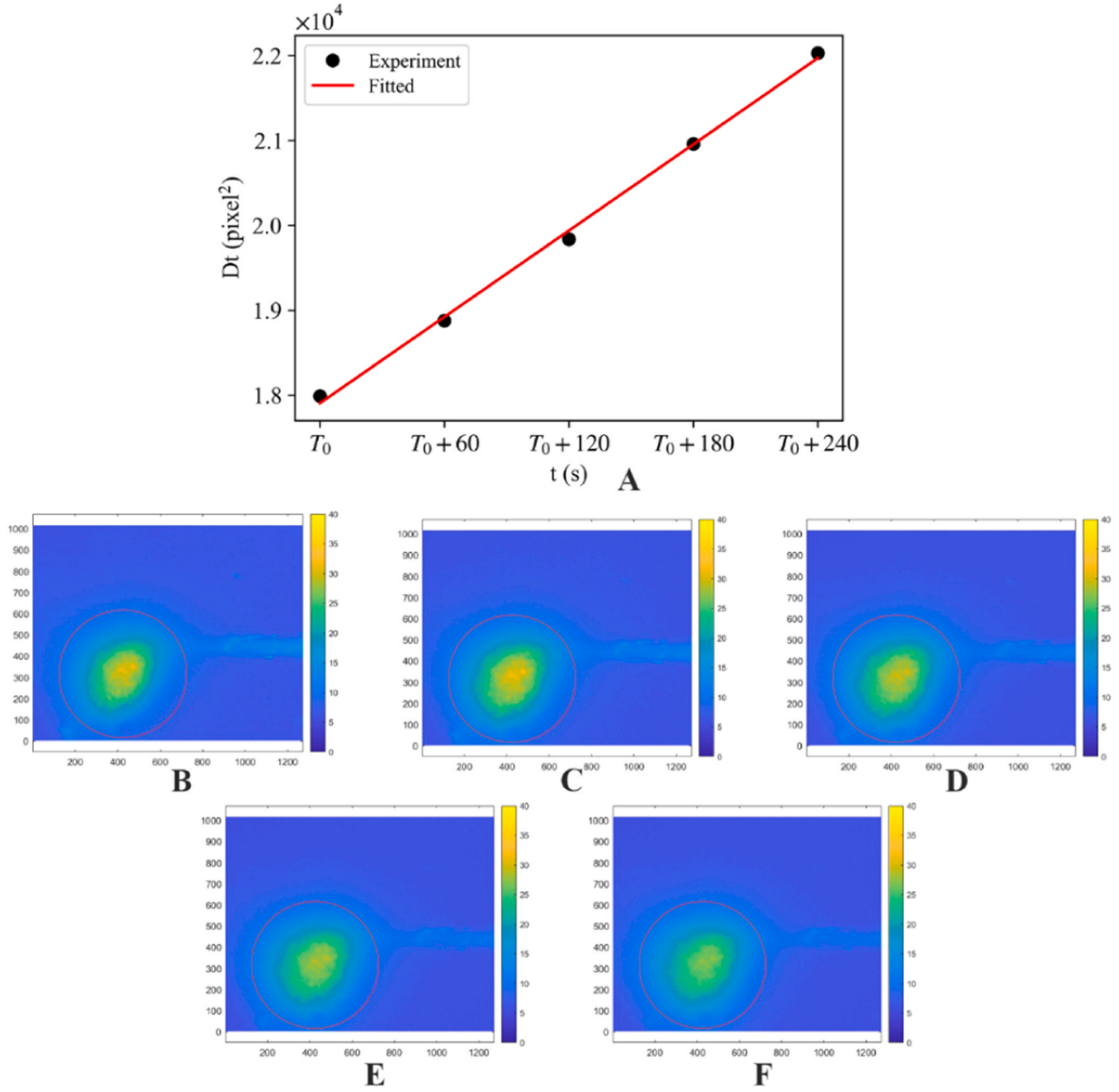

Fig. 6. Example of FITC@Fe_3O_4 diffusion in brain slices. A. Fitted FITC@Fe_3O_4 diffusion curve. B-F. Pictures taken continuously after FITC@Fe_3O_4 was injected into the brain slices (taken every 1 min, 1 pixel = 0.8 μm).

simulated. The results showed that the diffusion coefficients of NPs of various sizes in the ISS model were consistent in the three directions, as shown in Fig. 4. The diffusion of NPs in the selected ISS model was isotropic.

3.3. Effect of size on NP diffusion

In this experiment, uncharged NPs (2–35 nm) were simulated to diffuse in the ISS. For uncharged NPs, the particle size was negatively correlated with the diffusion coefficient; the larger the particle size, the slower was the diffusion. As the particle size increased, the diffusion coefficient decreased exponentially. The fitting curve and formula are shown in Fig. 5. The standard deviation of the diffusion coefficient of the small NPs was larger. The diffusion coefficient of the 2 nm NPs in the five ISS models ranged from 5.217 to 7.483 × 10^{-11} m^2/s. The differences in the diffusion coefficients of large NPs among the five ISS models were small. The diffusion coefficient of the 35 nm NPs in the five ISS models ranged from 0.149 to 0.235 × 10^{-11} m^2/s.

3.4. Diffusion of charged NPs

Fig. 6B-F shows the concentration field of FITC@Fe_3O_4 NPs in brain slices, which were derived from fluorescence images captured by a CCD camera. A few minutes after the injection, the FITC@Fe_3O_4 NPs reached a stable diffusion state. The first image was captured at T_0. Because T_0 is not a critical parameter for acquiring the diffusion coefficient, it is casual to determine the appropriate time. After the first image was captured, subsequent images were captured every 60 s. The diminished

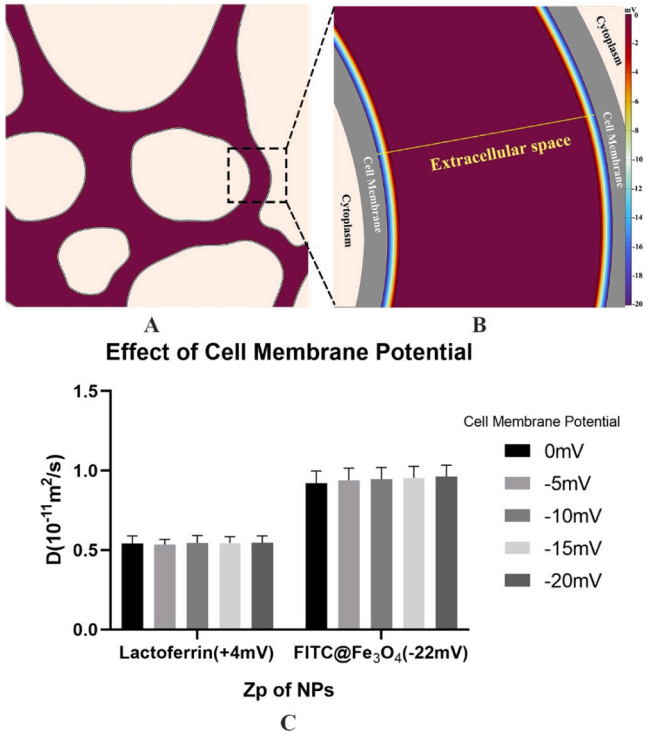

Fig. 7. Effect of cell membrane potential on charged nanoparticles (NPs) diffusion. A-B Cell membrane potential of the ISS model, B was the partial enlarged view. C. Diffusion coefficients of lactoferrin (+4 mV) and FITC@Fe_3O_4 (−22 mV) under different cell membrane potentials.

Table 1
Parameters.

Parameter	Value (Unit)
Temperature (T)	310.15 (K)
Boltzmann's constant (k_B)	1.38×10^{-23} (J/K)
Viscosity (Interstitial fluid)	3.0×10^{-3} (Pa.s)[25]
Vacuum permittivity (ϵ_0)	8.85×10^{-12} (C/Vm)
Elementary charge (e)	1.60×10^{-19} (C)
ion concentration (c)	0.154 (mol/L)[13]
Permittivity of normal saline (ϵ)	6.55×10^{-10} (C/Vm)[13]
Avogadro constant (N)	6.02×10^{23} (mol^{-1})

Table 2
Comparison of Simulation Results with Literature and Experimental Data.

Uncharged NP		Literature	Simulation
	d_H, nm	D, 10^{-11} m^2/s	D, 10^{-11} m^2/s
	2.95	5.36[9]	4.33 ± 0.74
	8.8	1.4[29]	1.01 ± 0.14
	13	0.78[29]	0.64 ± 0.08
	14.1	0.648[9]	0.58 ± 0.06
	35.4	0.0167[9]	0.20 ± 0.04
Charged NP	NP d_H, nm (Zp)	Literature and Experimental	Simulation
	Lactoferrin 9.2 (+4 mV)	0.58[29]	8.464 ± 1.637
	FITC@Fe_3O_4 20.41 (−22.4 mV)	1.09 ± 0.22	161.083 ± 15.786

fluorescence after NP injection is distinct, which was mainly due to diffusion. The concentration field, represented by the fluorescence intensity within the ROI, was interpolated using Eq. (11).

The interpolated parameter Dt over t is shown in Fig. 6A. Because the diffusion coefficient D was assumed to be constant, parameter Dt was fitted linearly to t. The slope of the fitted curve represents the diffusion coefficient of FITC@Fe_3O_4 NPs. The fitted slope was 16.93 $pixels^2/s$. Considering that 1 pixel corresponds to 0.8 μm, the diffusion coefficient of FITC@Fe_3O_4 NPs in brain slices was $1.09 \pm 0.22 \times 10^{-11}$ m^2/s (n = 4 slices).

The Zp of 9.2 nm lactoferrin is approximately + 4 mV [30], and the in vivo diffusion coefficient is 0.58×10^{-11} m^2/s [29]. The simulation results showed that the diffusion coefficients of lactoferrin and FITC@Fe_3O_4 were $8.464 \pm 1.637 \times 10^{-11}$ m^2/s and $1.611 \pm 0.158 \times 10^{-9}$ m^2/s, respectively. The simulated diffusion coefficients were 2–3 orders of magnitude higher than those reported in the literature and the experimental data, as shown in Table 2. From this, it can be speculated that there was something in the ISS that hindered the diffusion of charged NPs.

3.5. Effect of cell membrane potential on charged NPs diffusion

As discussed in Section 3.4, the diffusion of charged NPs in the ISS was hindered. Some studies have explored the diffusion of charged NPs in ECM matrigel and cross-linked hydrogels [14,31]. However, there are currently no studies that can quantify the selective filtering effect of electrostatic bandpass in ECM on charged substances. To study the effect of cell membrane potential on the diffusion of charged NPs, we adjusted the ECM viscosity of lactoferrin and FITC@Fe_3O_4 from 0.003 Pa·s to 0.1 Pa·s and 11 Pa·s, respectively, to simulate the hindered diffusion of charged NPs in the ECM. When the viscosity reached 0.1 Pa.s and 11 Pa.s, the diffusion coefficient of lactoferrin and FITC@Fe_3O_4 were $0.547 \pm 0.042 \times 10^{-11}$ m^2/s and $0.963 \pm 0.071 \times 10^{-11}$ m^2/s respectively, which was consistent with the experimental data and could be used in this part of the study. The initial resting state Zp of all cell membranes was set to − 20 mV [32],as shown in Fig. 7B. The Zp of the cell membrane range from − 20 mV to 0 mV. The Kruskal–Wallis test was performed using GraphPad Prism version 8.0.2 for Windows (GraphPad Software, Boston, Massachusetts, USA), and statistical significance was set at $p < 0.05$.

The results showed that there was no statistical difference in the diffusion coefficient of lactoferrin (+4 mV) under different cell membrane potentials ($P = 0.9924$). The diffusion coefficient of FITC@Fe_3O_4 (−22 mV) gradually increased with the increase of the absolute value of cell membrane potential. When the cell membrane potential was 0 mV, the diffusion coefficient of FITC@Fe_3O_4 was $0.922 \pm 0.076 \times 10^{-11}$ m^2/s. When the cell membrane potential was − 20 mV, the diffusion coefficient of FITC@Fe_3O_4 was $0.963 \pm 0.071 \times 10^{-11}$ m^2/s. However, the difference in the diffusion coefficient of FITC@Fe_3O_4 under different cell membrane potentials was not significant ($P = 0.9206$).

4. Discussion

The brain ISS is the last mile of drug delivery. The diffusion of drugs, including nanomedicines, is affected by both the drug and the ISS environment. Brain tissue can be considered as a random porous medium in which nerve cells and the ECM are viscoelastic solid components, and interstitial fluid is the pore fluid component [33]. The α and tortuosity (λ) of the ECS are the main factors that affect the diffusion of substances within it, among which λ includes the geometric path length, local dead-space microdomains, and the obstruction of substance diffusion by the ECM components [7]. To simulate the actual brain ISS environment as accurately as possible, the 2D brain ISS model in the present study was constructed from EM images obtained using high-pressure cryofixation. High-pressure cryofixation technology uses a combination of liquid nitrogen injection and very high pressure to preserve small samples instantly without the damage caused by the formation of ice crystals or shrinkage and deformation. Natalya et al. showed that, compared with high-pressure cryofixation, chemical fixation induced total volume shrinkage of the somatosensory neocortex by 30 % and reduced the extracellular volume by six times [17]. The

present study used manual sketching to extract the geometric outline of the ECS so that its geometric structure could be preserved as much as possible. This makes it extremely difficult to construct 3D models. Kinney et al. used a suite of tools to reconstruct the 3D geometry of 180 μm^3 rat CA1 hippocampal neuropil and corrected tissue shrinkage to reflect in vivo conditions. They reconstructed a 3D ECS and used Monte Carlo simulations to model small molecules diffusion within it. Since the outline of the extracellular plasma membrane was also manually traced, the 3D ECS constructed in that study was small. When performing small molecule diffusion simulations, the reconstructed size around the release point had to be artificially expanded eight times to improve the estimate of micron-scale tortuosity [34]. Although the ISS models in this study were 2D, the size of the ECS constructed could meet the stable diffusion of NPs and could easily realize the diffusion of NPs at different release points. Although dimensional shrinkage is applied in almost all areas of physical analysis to take advantage of uniformity along one or more directions, it can still cause bias in the results compared to three-dimensional models. The dimensionality of a model also plays an important role in effective diffusion. For isotropic porous media, the effective diffusion coefficient obtained from the 2D simulation is generally lower than that of the 3D model; however, the trend of the diffusion coefficient obtained under both conditions is consistent [35,36]. The present study validated the model by comparing simulation results with literature results and performed a simulation of the ISS model constructed based on multiplane reconstructed EM images to verify the isotropy of the model. The 2D ISS model constructed in this study satisfied the simulation requirements. To the best of our knowledge, this is the first simulation study of NP diffusion based on a model of actual extracellular space. We explored the effects of changes in the particle size, charge, and cell membrane potential on NP diffusion.

Particle size and Zp are important parameters of NPs and are the main factors affecting their diffusion in the brain ISS. Generally, the width of the ECS is 30–60 nm [6]. This is too small for most particulate drug delivery systems and viruses carrying therapeutic genes to effectively penetrate the brain parenchyma. However, Nance et al. found that NPs 114 nm in size, tightly packed with polyethylene glycol (PEG) can diffuse into the brain [37]. This enables the use of larger NPs to achieve effective drug delivery within the brain parenchyma. Although PEG coating can improve NP penetration, PEGylation has been shown to interfere with NP function [38]. In terms of applicability, the size range of the NPs simulated in this study was 2–35 nm. Diffusion coefficient has been shown to be negatively correlated with NP size [7,13,39]. The conclusions drawn in the present study are consistent with these findings. Because this study uses a 2D model, the simulated diffusion coefficients of small nanoparticles were smaller than the experimentally measured diffusion coefficients. This is because 3D models allow greater freedom of movement and more diffusion paths, and smaller particles may be more affected. The simulated result of the 35.4 nm NPs was higher than the experimental measurements, which might be because of neglecting the volume effect of the NPs. The width of the brain's ECS is on the nanoscale and is unsuitable for the diffusion of large particles. When the diameter of the NPs was less than 10 nm, the diffusion coefficient increased rapidly with decreasing particle size. When the diameter of the NPs was larger than 10 nm, although they could still diffuse, their speed slowed and tended to zero. Therefore, to realise efficient diffusion of NPs in the ISS, NPs with small particle sizes should be selected.

Zeta potential is an important parameter for characterising the stability of an NP dispersion system; the higher its absolute value, the more stable is the dispersion system. According to the classical Derjaguin, Landau, Verwey, and Overbeek theory, the total potential energy of the interaction between colloidal particles is equal to the sum of the van der Waals attractive potential energy and the electrostatic repulsive potential energy caused by the electric double layer. We adopted the research method of Yuan et al. to quantify the relationship between the Zp and δ_{eff} [13]. The results for the charged NPs revealed a significant difference between the simulated results and experimental data, and the simulated diffusion coefficient was significantly higher than the experimentally measured value. Therefore, it can be speculated that there is something in the ECM that hinders the diffusion of charged NPs. Studies have shown that ECM components (mainly heparan sulphate chains) can significantly inhibit the diffusive motion of charged species [10,29,40]. The results of the present study agree with this view.

Under physiological conditions, neurones undergo a series of changes in depolarisation, followed by hyperpolarisation during excitation. In pathological states such as cerebral ischemia, migraine aura, and seizures, a wave of sustained depolarisation occurs in the cerebral cortex [41]. The membrane potential at which sustained depolarisation occurs drops from − 70 mV to 0 mV [42]. In the present study, the diffusion of charged NPs in the ISS was simulated in a state of diffuse cell depolarisation. Simulation studies showed that there was no statistical difference in the diffusion coefficients of lactoferrin (+4 mV) and FITC@Fe_3O_4 (−22 mV) under different cell membrane potentials. Changes in the cell membrane potential had little effect on the diffusion coefficient of charged NPs. It is likely that the insignificant effect of the cell membrane potential on charged NPs was because of the small effective area of the membrane potential. Only when the NPs move to the vicinity of the cell membrane are they affected by the cell membrane; therefore, the cell membrane potential has a limited effect on the diffusion of NPs. It should be noted that the present study did not consider the phagocytosis of NPs by cells or the effect of charged NPs on the cell membrane.

The brain ISS changes under different physiological and pathological states. The ECS of neonatal mammals accounts for approximately 40 % of the total brain volume, and its proportion gradually decreases with age [43]. In malignant gliomas, several ECM components are upregulated in the tumour itself and at the tumour boundary to promote tumour invasion [44]. After cerebral ischemia, a series of changes occurs in the ISS, including degradation of the basement membrane [45], depolarisation of nerve cells [46], and reduction in the extracellular space to 5 % of the total brain volume [47]. During the development of Alzheimer's disease, the expression of ECM components in the brain changes, further aggravating the pathological process [48]. In the future, we will include pathological changes in the ISS in our research and explore the diffusion of NPs. This study has some limitations and shortcomings. First, the ISS models constructed in this study was derived from EM images of a mouse. Second, the ISS models constructed in this study were two-dimensional. Finally, whether the conclusions of this study are applicable to NPs larger than 35 nm is unknown. In the future, we will further expand the scale of the model, try to construct 3D ISS models and ISS models under different pathological conditions, and explore the diffusion rules of NPs.

5. Conclusion

In this study, five 2D ISS models were constructed based on EM images to preserve the actual ECS of the brain. A particle tracing model was used to simulate the diffusion of the NPs. The models were validated by comparison with data from the literature and demonstrated that NP diffusion within the grey matter is isotropic. The effect of the particle size on the diffusion coefficient of the NPs was explored by numerical simulation. By comparing the literature and experimental data with numerical simulation results, the diffusion of charged NPs within the ISS was explored, and the effect of changes in the cell membrane potential on the diffusion of charged NPs was further investigated.

This study found that in the ISS, 1) the diffusion coefficient increased rapidly with decreasing NP size, 2) the diffusion of charged NPs was hindered, and 3) the cell membrane potential had little effect on the diffusion of charged NPs.

To achieve the efficient diffusion of NPs in the brain ISS, small uncharged NPs should be selected. This study contributes to the design and development of nanomedicines for the treatment of brain diseases.

Funding

This work was supported by the National Natural Science Foundation of China (No. 81771790).

CRediT authorship contribution statement

Peiqian Chen: Writing – original draft, Software, Methodology, Conceptualization. **Weiwu Yao:** Writing – review & editing, Funding acquisition. **Bing Dong:** Formal analysis, Data curation.

Declaration of Competing Interest

The authors declare that the research was conducted in the absence of any commercial or financial relationships that could be construed as a potential conflict of interest.

Data Availability Statement

The simulation cases used to support the findings of this study were supplied by Weiwu Yao under license. Requests for access to these data should be made to Weiwu Yao, yaoweiwuhuan@ 163.com. In addition, a typical case of numerical simulation was shared on Mendeley Data (https://data.mendeley.com/datasets/5s7d352n2r/1).

Acknowledgements

We would like to thank the research group of Professor Guoyuan Yang, School of Biomedical Engineering, Shanghai Jiao Tong University, for providing the equipment and guidance needed for the experiment.

Appendix A. Supporting information

Supplementary data associated with this article can be found in the online version at doi:10.1016/j.csbj.2024.06.002.

References

[1] Zhao Q, Cheng N, Sun X, Yan L, Li W. The application of nanomedicine in clinical settings. Front Bioeng Biotechnol 2023;vol. 11:1219054. https://doi.org/10.3389/fbioe.2023.1219054.
[2] Siddique S, Chow JCL. Application of nanomaterials in biomedical imaging and cancer therapy. Nanomaterials 2020;vol. 10(9):1700. https://doi.org/10.3390/nano10091700.
[3] Siddique S, Chow JCL. Recent advances in functionalized nanoparticles in cancer theranostics. Nanomaterials 2022;vol. 12(16):2826. https://doi.org/10.3390/nano12162826.
[4] Zhang X, Zhou J, Gu Z, Zhang H, Gong Q, Luo K. Advances in nanomedicines for diagnosis of central nervous system disorders. Biomaterials 2021;vol. 269:120492. https://doi.org/10.1016/j.biomaterials.2020.120492.
[5] Soni S, Ruhela RK, Medhi B. Nanomedicine in Central Nervous System (CNS) Disorders: A Present and Future Prospective. Adv Pharm Bull 2016;vol. 6(3):319–35. https://doi.org/10.15171/apb.2016.044.
[6] Sun Y, Sun X. Exploring the interstitial system in the brain: the last mile of drug delivery. Rev Neurosci 2021;vol. 32(4):363–77. https://doi.org/10.1515/revneuro-2020-0057.
[7] Syková E, Nicholson C. Diffusion in brain extracellular space. Physiol Rev 2008;vol. 88(4):1277–340. https://doi.org/10.1152/physrev.00027.2007.
[8] Lei Y, Han H, Yuan F, Javeed A, Zhao Y. The brain interstitial system: Anatomy, modeling, in vivo measurement, and applications. Prog Neurobiol 2017;vol. 157:230–46. https://doi.org/10.1016/j.pneurobio.2015.12.007.
[9] Thorne RG, Nicholson C. *In vivo* diffusion analysis with quantum dots and dextrans predicts the width of brain extracellular space. Proc Natl Acad Sci USA 2006;vol. 103(14):5567–72. https://doi.org/10.1073/pnas.0509425103.
[10] Lieleg O, Baumgärtel RM, Bausch AR. Selective Filtering of Particles by the Extracellular Matrix: An Electrostatic Bandpass. Biophys J 2009;vol. 97(6):1569–77. https://doi.org/10.1016/j.bpj.2009.07.009.
[11] Warren EAK, Payne CK. Cellular binding of nanoparticles disrupts the membrane potential. RSC Adv 2015;vol. 5(18):13660–6. https://doi.org/10.1039/C4RA15727C.
[12] Dante S, et al. Selective targeting of neurons with inorganic nanoparticles: revealing the crucial role of nanoparticle surface charge. ACS Nano 2017;vol. 11(7):6630–40. https://doi.org/10.1021/acsnano.7b00397.
[13] T. Yuan, L. Gao, W. Zhan, and D. Dini, "Effect of Particle Size and Surface Charge on Nanoparticles Diffusion in the Brain White Matter," Pharm Res, vol. 39, no. 4, pp. 767–781, Apr. 2022, doi: 10.1007/s11095–022-03222–0.
[14] Hansing J, Ciemer C, Kim WK, Zhang X, DeRouchey JE, Netz RR. Nanoparticle filtering in charged hydrogels: Effects of particle size, charge asymmetry and salt concentration. Eur Phys J E 2016;vol. 39(5):53. https://doi.org/10.1140/epje/i2016-16053-2.
[15] Holter KE, et al. Interstitial solute transport in 3D reconstructed neuropil occurs by diffusion rather than bulk flow. Proc Natl Acad Sci USA 2017;vol. 114(37):9894–9. https://doi.org/10.1073/pnas.1706942114.
[16] Jin B-J, Smith AJ, Verkman AS. Spatial model of convective solute transport in brain extracellular space does not support a 'glymphatic' mechanism. J Gen Physiol 2016;vol. 148(6):489–501. https://doi.org/10.1085/jgp.201611684.
[17] Korogod N, Petersen CC, Knott GW. Ultrastructural analysis of adult mouse neocortex comparing aldehyde perfusion with cryo fixation. eLife 2015;vol. 4:e05793. https://doi.org/10.7554/eLife.05793.
[18] Tsang TK, et al. High-quality ultrastructural preservation using cryofixation for 3D electron microscopy of genetically labeled tissues. eLife 2018;vol. 7:e35524. https://doi.org/10.7554/eLife.35524.
[19] Ge Z, Wang Y. Estimation of nanodiamond surface charge density from zeta potential and molecular dynamics simulations. J Phys Chem B 2017;vol. 121(15):3394–402. https://doi.org/10.1021/acs.jpcb.6b08589.
[20] Bhattacharjee S, Elimelech M. Surface Element Integration: A Novel Technique for Evaluation of DLVO Interaction between a Particle and a Flat Plate. J Colloid Interface Sci 1997;vol. 193(2):273–85. https://doi.org/10.1006/jcis.1997.5076.
[21] Banerjee S, Nayak AK, Sen KK. Aquasomes: a nanoparticulate approach for therapeutic applications. *Systems of Nanovesicular Drug Delivery*. Elsevier,; 2022. p. 207–19. https://doi.org/10.1016/B978-0-323-91864-0.00025-5.
[22] Lin X, Wang C, Wang M, Fang K, Gu N. Computer Simulation of the Effects of Nanoparticles' Adsorption on the Properties of Supported Lipid Bilayer. J Phys Chem C 2012;vol. 116(33):17960–8. https://doi.org/10.1021/jp305784z.
[23] Nangia S, Sureshkumar R. Effects of nanoparticle charge and shape anisotropy on translocation through cell membranes. Langmuir 2012;vol. 28(51):17666–71. https://doi.org/10.1021/la303449d.
[24] Su D, Ma R, Salloum M, Zhu L. Multi-scale study of nanoparticle transport and deposition in tissues during an injection process. Med Biol Eng Comput 2010;vol. 48(9):853–63. https://doi.org/10.1007/s11517-010-0615-0.
[25] Bera K, et al. Extracellular fluid viscosity enhances cell migration and cancer dissemination. Nature 2022;vol. 611(7935):365–73. https://doi.org/10.1038/s41586-022-05394-6.
[26] Wang T, Kass IS. Preparation of Brain Slices. *Neurotransmitter Methods*, vol. 72. New Jersey: Humana Press,; 1997. p. 1–14. https://doi.org/10.1385/0-89603-394-5:1.
[27] Brenig W. Brownian Motion: Langevin Equation. *Statistical Theory of Heat*. Berlin, Heidelberg: Springer Berlin Heidelberg,; 1989. p. 69–72. https://doi.org/10.1007/978-3-642-74685-7_14.
[28] Gorenflo R, Mainardi F. Random walk models approximating symmetric space-fractional diffusion processes. In: Elschner J, Gohberg I, Silbermann B, editors. *Problems and Methods in Mathematical Physics*. Basel: Birkhäuser Basel; 2001. p. 120–45. https://doi.org/10.1007/978-3-0348-8276-7_10.
[29] Thorne RG, Lakkaraju A, Rodriguez-Boulan E, Nicholson C. *In vivo* diffusion of lactoferrin in brain extracellular space is regulated by interactions with heparan sulfate. Proc Natl Acad Sci USA 2008;vol. 105(24):8416–21. https://doi.org/10.1073/pnas.0711345105.
[30] Pryshchepa O, Sagandykova G, Rudnicka J, Pomastowski P, Sprynskyy M, Buszewski B. Synthesis and physicochemical characterization of zinc-lactoferrin complexes. J Dairy Sci 2022;vol. 105(3):1940–58. https://doi.org/10.3168/jds.2021-20538.
[31] Lieleg O, Baumgärtel RM, Bausch AR. Selective filtering of particles by the extracellular matrix: an electrostatic bandpass. Biophys J 2009;vol. 97(6):1569–77. https://doi.org/10.1016/j.bpj.2009.07.009.
[32] Guy Y, Sandberg M, Weber SG. Determination of ζ-Potential in Rat Organotypic Hippocampal Cultures. Biophys J 2008;vol. 94(11):4561–9. https://doi.org/10.1529/biophysj.107.112722.
[33] Comellas E, Budday S, Pelteret J-P, Holzapfel GA, Steinmann P. Modeling the porous and viscous responses of human brain tissue behavior. Comput Methods Appl Mech Eng 2020;vol. 369:113128. https://doi.org/10.1016/j.cma.2020.113128.
[34] Kinney JP, Spacek J, Bartol TM, Bajaj CL, Harris KM, Sejnowski TJ. Extracellular sheets and tunnels modulate glutamate diffusion in hippocampal neuropil. J Comp Neurol 2013;vol. 521(2):448–64. https://doi.org/10.1002/cne.23181.
[35] S. Trinh, P. Arce, and B.R. Locke, "Effective Diffusivities of Point-Like Molecules in Isotropic Porous Media by Monte Carlo Simulation".
[36] Dartois A, Beaudoin A, Huberson S. Impact of local diffusion on macroscopic dispersion in three-dimensional porous media. Comptes Rendus Mécanique 2018;vol. 346(2):89–97. https://doi.org/10.1016/j.crme.2017.12.012.
[37] Nance EA, et al. A Dense Poly(Ethylene Glycol) Coating Improves Penetration of Large Polymeric Nanoparticles Within Brain Tissue (Aug.) Sci Transl Med 2012;vol. 4(149). https://doi.org/10.1126/scitranslmed.3003594 (Aug.).
[38] Wu JR, Hernandez Y, Miyasaki KF, Kwon EJ. Engineered nanomaterials that exploit blood-brain barrier dysfunction for delivery to the brain. Adv Drug Deliv Rev 2023;vol. 197:114820. https://doi.org/10.1016/j.addr.2023.114820.
[39] Yuan T, Yang Y, Zhan W, Dini D. Mathematical Optimisation of Magnetic Nanoparticle Diffusion in the Brain White Matter. IJMS 2023;vol. 24(3):2534. https://doi.org/10.3390/ijms24032534.
[40] Le Goas M, et al. How Do Surface Properties of Nanoparticles Influence Their Diffusion in the Extracellular Matrix? A Model Study in Matrigel Using Polymer-

Grafted Nanoparticles. Langmuir 2020;vol. 36(35):10460–70. https://doi.org/10.1021/acs.langmuir.0c01624.
[41] Taş YÇ, Solaroğlu İ, Gürsoy-Özdemir Y. "Spreading depolarization waves in neurological diseases: a short review about its pathophysiology and clinical relevance,". CN 2019;vol. 17(2):151–64. https://doi.org/10.2174/1570159×15666170915160707.
[42] Kramer DR, Fujii T, Ohiorhenuan I, Liu CY. Cortical spreading depolarization: Pathophysiology, implications, and future directions. J Clin Neurosci 2016;vol. 24:22–7. https://doi.org/10.1016/j.jocn.2015.08.004.
[43] Tønnesen J, Hrabětová S, Soria FN. Local diffusion in the extracellular space of the brain. Neurobiol Dis 2023;vol. 177:105981. https://doi.org/10.1016/j.nbd.2022.105981.
[44] Ferrer VP, Moura Neto V, Mentlein R. Glioma infiltration and extracellular matrix: key players and modulators. Glia 2018;vol. 66(8):1542–65. https://doi.org/10.1002/glia.23309.
[45] Kang M, Yao Y. Basement membrane changes in ischemic stroke. Stroke 2020;vol. 51(4):1344–52. https://doi.org/10.1161/STROKEAHA.120.028928.
[46] Andrew RD, et al. The Critical Role of Spreading Depolarizations in Early Brain Injury: Consensus and Contention. Neurocrit Care 2022;vol. 37(S1):83–101. https://doi.org/10.1007/s12028-021-01431-w.
[47] Vořísek I, Syková E. Ischemia-Induced Changes in the Extracellular Space Diffusion Parameters, K^+, and pH in the Developing Rat Cortex and Corpus Callosum. J Cereb Blood Flow Metab 1997;vol. 17(2):191–203. https://doi.org/10.1097/00004647-199702000-00009.
[48] Sun Y, et al. Role of the Extracellular Matrix in Alzheimer's Disease. Front Aging Neurosci 2021;vol. 13:707466. https://doi.org/10.3389/fnagi.2021.707466.